Journal of Solid State Electrochemistry
https://doi.org/10.1007/s10008-023-05392-2

ORIGINAL PAPER

# Electrochemical sensors based on antimony tin oxide-Prussian blue screen-printed electrode and PEDOT-Prussian blue for potassium ion detection

**Sorina Alexandra Leau[1,4] · Cecilia Lete[1] · Mariana Marin[1] · Francisco Javier del Campo[2,3] · Ioana Diaconu[4] · Stelian Lupu[4]**

Received: 30 September 2022 / Revised: 15 December 2022 / Accepted: 10 January 2023


**Abstract**
The development and analytical applications of electrochemical sensors based on antimony tin oxide (ATO)–Prussian blue (PB) screen-printed electrode (SPE) and PEDOT-PB modified glassy carbon electrode are presented. The ATO-PB electrode was successfully applied in the electrochemical detection of $K^+$ ions. The detection and quantification limits value of 1.1 mM and of 3.7 mM, respectively, have been obtained. A high sensitivity of 0.035 A $M^{-1}$ $cm^{-2}$ has been also obtained. In addition, a sensing material based on poly(3,4-ethylenedioxythiophene) (PEDOT) and PB has been developed by a sinusoidal voltage electrochemical procedure and tested toward the potassium ion detection. The PEDOT-PB sensing material displayed the characteristic redox wave of the PB component and good analytical performance toward potassium ion detection. These results demonstrate the utility of the novel electrode materials in the development of electrochemical sensors for electroinactive analytes.

**Keywords** Antimony tin oxide · Prussian blue · Potassium ion · Screen-printed electrodes · Sinusoidal voltage · Electrochemical sensor

## Introduction

Screen-printed electrodes (SPEs) have emerged in the last decades as outstanding enablers of various commercial electrochemical sensors and biosensors. SPEs display several unique properties like reproducibility, mass production, reliability, potential of miniaturization, and low cost, which ensured their successful use in various electrochemical (bio)sensors applications [1]. In addition, their versatile modification with various inorganic and organic materials, synthetic and biologic recognition elements, open the way to new applications in biomedical, food, and environmental fields [2–4]. The use of carbonaceous materials such as carbon nanotubes and graphene, metallic nanoparticles, and inorganic mediators like Prussian Blue (PB) in the SPEs modification has been successfully demonstrated in many applications [5–7]. The combination of various modifiers could provide synergistic effects that improve the selectivity

✉ Cecilia Lete
clete@icf.ro

✉ Francisco Javier del Campo
javier.delcampo@bcmaterials.net

✉ Stelian Lupu
stelian.lupu@upb.ro

Sorina Alexandra Leau
sleau@icf.ro

Mariana Marin
mmaria@icf.ro

Ioana Diaconu
ioana.diaconu@upb.ro

[1] Institute of Physical Chemistry, Ilie Murgulescu" of the Romanian Academy, 202 Splaiul Independentei, Bucharest 060021, Romania

[2] BCMaterials, Basque Center for Materials, Applications and Nanostructures, UPV/EHU Science Park, Leioa 48940, Spain

[3] Ikerbasque Basque Foundation for Science, Plaza Euskadi 5, Bilbao 48009, Spain

[4] Department of Analytical Chemistry and Environmental Engineering, Faculty of Chemical Engineering and Biotechnologies, University Politehnica of Bucharest, 1-7 Gh. Polizu Street, Bucharest 011061, Romania

Published online: 20 January 2023

and the sensitivity, expanding in this way the potential use of modified SPEs. Conducting antimony tin oxide (ATO) microparticles present a light gray color that makes them suitable candidates for spectroelectrochemical applications [8]. The spectroelectrochemical measurements provide additional structural information upon the controlled changed of the electrode potential. The grafting of molecular species on transparent electrodes reveals potential applications in electrocatalysis, optoelectronic devices, and provided useful information related to the stability and structure of the resulting interface. The incorporation of ATO microparticles in screen-printable inks ensures the development of flexible electrochromic devices [9–11]. The integration of Prussian blue modified SPEs into spectroelectrochemical applications further expanded their use in biosensors technology [12]. Prussian blue is a mixed valence transition metal hexacyanoferrate, namely ferric ferrocyanide, with formula $Fe_4^{III}[Fe^{II}(CN)_6]_3$ and characterized by a cubic lattice. The PB electrochemical behavior consists in two redox waves, namely the reduction of PB to the colorless reduced form Everitt's salt (ES), $K_4Fe_4^{II}[Fe^{II}(CN)_6]_3$, and the oxidation of PB to the yellowish oxidized form Berlin Green (BG), with formula $Fe^{III}[Fe^{III}(CN)_6]$ [13]. PB has been extensively prepared as thin films onto solid electrode substrates like noble metals or semiconductors by chemical and electrochemical methods for applications in (bio)sensors and energy storage applications [14–22]. Recently, the development of printing inks and materials and their integration into screen-printed electrodes have expanded the use of PB mainly in form of nanoparticles for various sensing strategies [23–25]. PB displays excellent electrochromic properties that have been already exploited in biosensing [26, 27]. In addition, the electrocatalytic properties of PB could also be exploited in the detection of electroactive analytes, for instance hydrogen peroxide, and the synergism between the electrochromic and electrocatalytic properties opens new potential applications. In this sense, the ATO nanoparticles have been coated with a nanometric layer of PB developing a new ink material for the design of novel screen-printed electrodes [12]. The ATO-PB-SPE devices displayed good electron transfer properties that make them suitable for electroanalytical applications.

In this work, the ATO-PB-SPE devices have been characterized by cyclic voltammetry and electrochemical impedance spectroscopy in $K^+$ containing aqueous solutions aiming to investigate the electron transfer capability and ionic conductivity. The influence of $K^+$ ions concentrations onto the reversible behavior of the PB/ES redox system has been studied. The dependence of the peak's potentials and currents of the PB/ES redox wave on $K^+$ ions concentration has been established. The possibility of the detection of electroinactive analytes like $K^+$ ions has been demonstrated. The comparison of the analytical performance of the ATO-PB sensing material with another sensing element composed of poly(3,4-ethylenedioxythiophene) (PEDOT) and PB has been performed. The PEDOT-PB composite material is prepared by a novel procedure based on the use of sinusoidal voltage superimposed on a constant potential. The PEDOT-PB composite material displayed the characteristic redox wave of the PB component. The combination of ATO nanoparticles and PB provided interesting results regarding the development of a novel electrode material with applications in the sensing of electro-inactive analytes with good analytical performance.

## Experimental section

### Reagents

Potassium chloride (Sigma-Aldrich), potassium nitrate (Sigma-Aldrich), sodium acetate (Sigma-Aldrich), glacial acetic acid (Sigma-Aldrich), monobasic potassium phosphate (Sigma-Aldrich), and dibasic potassium phosphate (Sigma-Aldrich) were of analytical grade. 3,4-ethylenedioxythiophene, iron (III) chloride, and potassium ferricyanide were purchased from Sigma-Aldrich. The aqueous solutions were prepared using double distilled water.

### Electrochemical measurements

The production of the Prussian Blue on ATO pastes and electrodes has been reported elsewhere [12, 28] but a summary will be given next for convenience. 20 g of ATO coated silica microparticles (1610-S, Milliken, BE) were suspended under vigorous magnetic stirring in 200 mL of a 25 mM Iron (II) sulfate solution. Next, 30 mL of 60 mM potassium hexacyanoferrate (III) were added slowly to the stirred solution. Prussian Blue was formed instantly on the surface of the $ATOSiO_2$ particles which, after reaction, were separated by decantation, washed with warm dilute HCl, and dried overnight in at 100 °C in an oven. The dried cake was ground to a fine powder using a mortar and pestle. The paste was subsequently produced by combination of this powder with a nitrocellulose binder solution. The nitrocellulose binder solution consisted nitrocellulose (Walsroder™ Nitrocellulose A400 ISO 30%, DuPont, DE) at 20% by weight in 2-butoxyethylethanol (ACROS, ES). The optimum relation of particles to nitrocellulose in the final paste was 2.5:1. The paste was homogenized using a three-roll mill to break up any lumps and ensure a particle size no larger than 10 microns in the final paste. Electrodes were screen printed using a manual press through 90 thread $cm^{-1}$ mesh screens as described before. The graphite electrodes were screen printed using C2030519P4 Graphite paste from Sun Chemical, ES.

The electrochemical experiments were carried out using the ATO-PB-SPE working electrode (geometric area of 0.071 $cm^{-2}$) connected via a Dropsens connector to an Autolab potentiostat/galvanostat 302 N (Ecochemie, The Netherlands). The potentiostat contains the FRA2 module and was connected to a PC and controlled by the GPES software, version 4.9 (Autolab, Ecochemie). The ATO-PB-SPE device contained also a pseudo-reference electrode $Ag/Ag^+$ and a graphite auxiliary electrode. All the potential values are expressed versus the $Ag/Ag^+$ pseudo-reference electrode. The ATO-PB-SPE electrodes were conditioned in 0.1 M KCl solution by means of cyclic voltammetric measurements in the potential range from 0.0 to 1.0 V vs. $Ag/Ag^+$ at a 50 mV $s^{-1}$ potential scan rate for 5 cycles in order to ensure the equilibration of the PB crystal structure with $K^+$ ions from the supporting electrolyte solution. Electrochemical impedance measurements were performed using the FRA2 module of the potentiostat at applied potential values of 0.14 V vs. $Ag/Ag^+$ and 0.82 V vs. $Ag/Ag^+$, using an excitation sin wave of 5 mV (rms) amplitude over the frequency range from 100 kHz to 0.01 Hz, in 0.1 M KCl aqueous solution. The electrochemical characterization and the analytical applications were performed by dropping a volume of 100 µL of the test solution onto the ATO-PB-SPE devices and carefully checking the full coverage of the entire active area of the electrodes.

The electrochemical behavior of ATO-PB-SPE device was compared to that of a glassy carbon electrode modified with a composite material consisting of poly(3,4-ethylenedioxythiophene) (PEDOT) organic conducting polymer and PB. The PEDOT-PB coating was prepared onto a glassy carbon disk electrode (GCE), with a diameter of 3 mm, in two steps using a sinusoidal voltage (SV) preparation procedure: i) the electropolymerization of the 3,4-ethylenedioxytiophene (EDOT) monomer was carried out from an aqueous solution of 10 mM EDOT and 25 mM $K_3Fe(CN)_6$ by applying a constant potential of 0.60 V vs. Ag/AgCl/KCl (3 M) reference electrode for a electrodeposition time of 1200 s. A sinusoidal voltage with amplitude of 0.35 V and frequency of 50 mHz was superimposed onto the constant potential of 0.60 V vs. Ag/AgCl/KCl (3 M). The coating was denoted as PEDOT-FeCN. ii) the GCE modified by PEDOT-FeCN coating was immersed in an aqueous solution containing 50 mM $FeCl_3$, and 0.1 M KCl, and a constant potential of 0.60 V vs. Ag/AgCl/KCl (3 M) reference electrode was applied for an electrodeposition time of 1200 s. A sinusoidal voltage with amplitude of 0.35 V and 50 mHz frequency was applied over the constant potential. The in-situ formation of PB takes place during the second preparation step. The modified electrode was denoted as PEDOT-PB-GCE.

The surface morphology of the working electrodes was assessed by scanning electron microscopy (FEG-SEM Hitachi S-4800) at 15 kV.

### Analytical measurements

The determination of potassium ions has been done by using the calibration plot protocol. In this sense, a series of potassium standard solutions with concentrations ranging from 0.1 to 10 mM were prepared. Then, a volume of 100 µL from each standard solution was dropped onto the SPE device surface ensuring the full coverage of the electrodes. Afterwards, the cyclic voltammetric signal was recorded at various potential scan rates. The PEDOT-PB-GCE device was used in the electrochemical and analytical measurements in connection with a Ag/AgCl/KCl (3 M) reference electrode and a glassy carbon rod as counter electrode, respectively.

## Results and discussion

### Electrochemical characterization of ATO-PB-SPE

The electrochemical properties and performance of ATO-PB-SPE devices have been investigated by using cyclic voltammetry (CV) in 0.1 M KCl aqueous supporting electrolyte solution. The presence of $K^+$ ions in solution is of paramount importance for the proper functioning of PB. The electrochemical reduction of PB to ES can be described by the following scheme reaction:

$$PB + K^+ + e^- \Leftrightarrow ES \quad (1)$$

The reduction process of PB is accompanied by the insertion of $K^+$ ions into the PB lattice, while the oxidation of ES back to PB is characterized by the rejection of $K^+$ ions. Consequently, the presence of $K^+$ ions into the electrolyte solution is required for the proper functioning of PB and this is the basic principle ensuring the development of an electrochemical sensor for $K^+$ ions. Figure 1A shows typical CVs recorded at ATO-PB-SPE in 0.1 M KCl solution at various potential scan rates ranging from 10 to 500 mV/s. The well-defined redox waves ascribed to PB/ES and PB/BG reversible transitions are visible at ca. 0.11 V vs. $Ag/Ag^+$ and 0.85 V vs. $Ag/Ag^+$, respectively.

There is an increase of both anodic and cathodic peak currents with the square root of the potential scan rate for the two redox waves, PB/ES and PB/BG, respectively, as can be seen in Fig. 1B. The reduction of PB to ES requires the ingress of $K^+$ ions from the electrolyte solution into the PB lattice, while the oxidation of ES form back to PB involves the expulsion of the $K^+$ ions. At the time scale of the CV experiments, the redox reaction of the PB/ES couple is a process controlled by the diffusion of $K^+$ ions. Further confirmation to a diffusion-controlled process is provided by the slope value of the *log (Ip)* versus *log* (*v)*

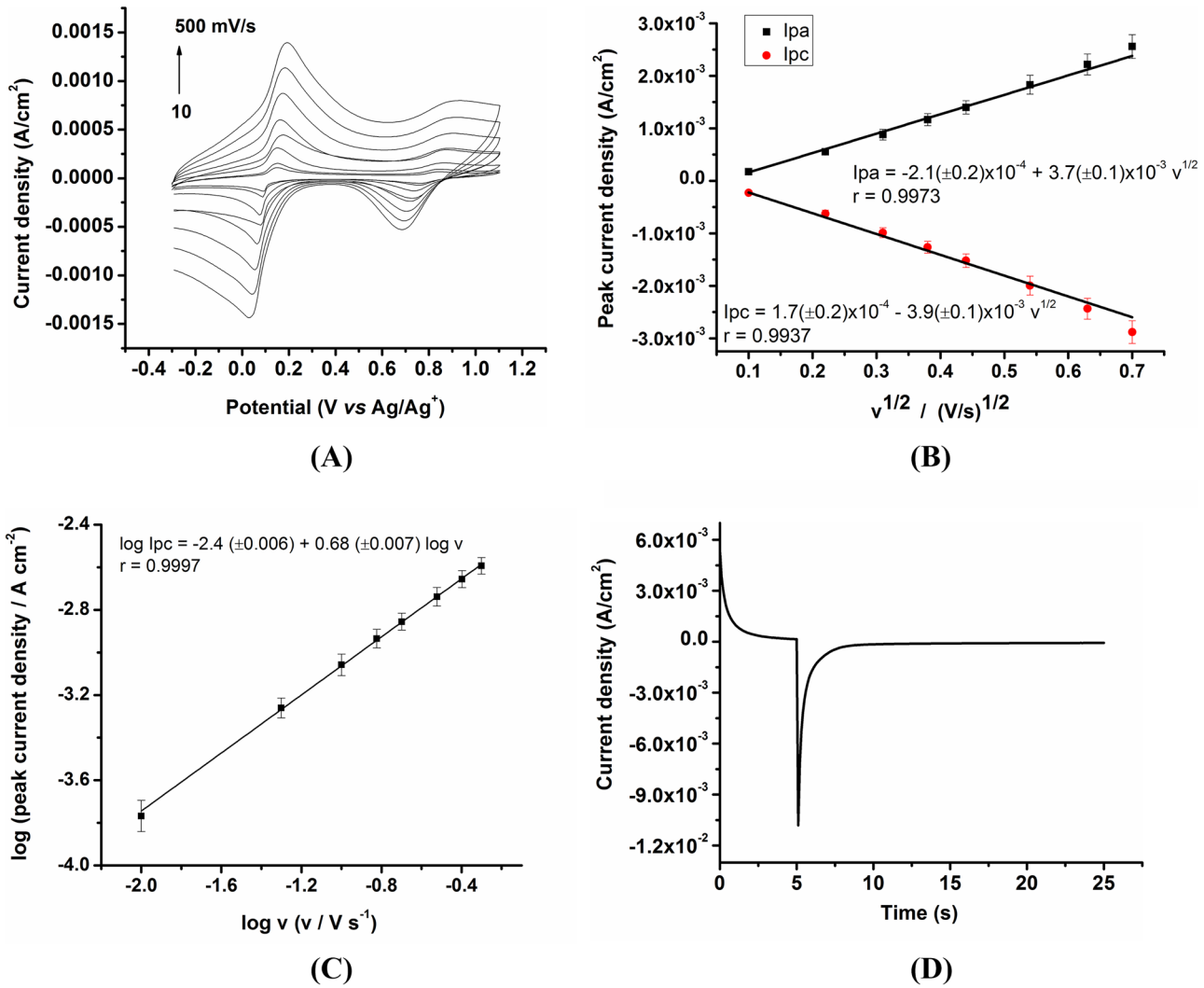


**Fig. 1** **A** CVs recorded at ATO-PB-SPE in 0.1 M KCl aqueous solution at different potential scan rates ranging from 10 to 500 mV/s. **B** The dependence of the anodic and cathodic peak current densities on the potential scan rate for PB/ES redox system. **C** Plot of the logarithm of the cathodic peak current density versus the logarithm of the potential scan rate for the PB/ES redox system. **D** Double step chronoamperogram recorded at ATO-PB-SPE in 0.1 M KCl. Applied potentials: $E_1 = +0.3$ V vs. $Ag/Ag^+$, $t_1 = 5$ s; $E_2 = (-0.3)$ V vs. $Ag/Ag^+$, $t_2 = 25$ s.

plot, when a value of 0.60 was obtained (see Fig. 1C). There is a strong correlation as shown by the high correlation coefficient value of 0.9997 that has been obtained. A similar value of the slope for the anodic peak current was obtained. These results demonstrate the fast transfer of electrons within the ATO-PB electrode material at the time scale of the experiment and the diffusion limited feature of the redox process. This behavior is fostering the development of an electrochemical sensor for the target analyte, i.e., $K^+$ ions. In addition, the surface coverage, $\Gamma$, of PB was estimated from the electrical charge (see Fig. 1D) consumed in the reduction of PB to ES (3.27 mC $cm^{-2}$) and a value of $3.4 \times 10^{-8}$ mol $cm^{-2}$ has been obtained. This surface coverage value points out to the high amount of immobilized PB onto $SiO_2$-ATO nanoparticles, which is favorable from the point of view of analytical applications where the loading of electroactive materials strongly influences the performance of the developed sensors. An estimation of the PB thickness ($l$) could be made on the assumption that the obtained PB surface coverage refers to a PB layer deposited over a flat disk electrode. In this case, the thickness of the PB layer could be calculated by using the formula [29]:

$$l = \frac{\Gamma\, a^3 N_A}{4} \tag{2}$$

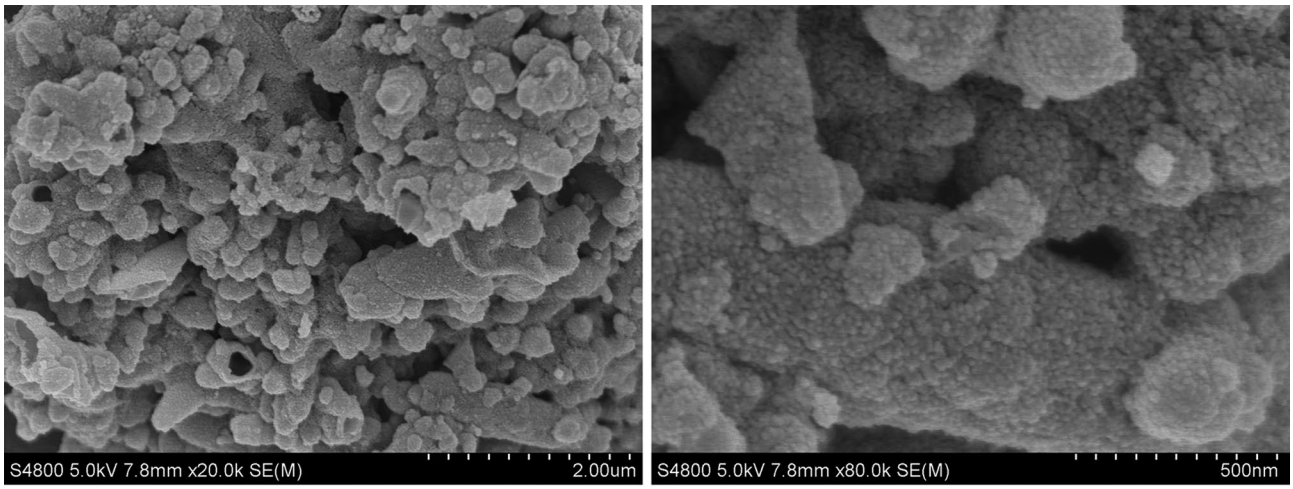


**Fig. 2** SEM images of ATO-PB materials at various magnifications: **A** 20 k and **B** 80 k

where $a$ is the unit cell of PB lattice (1.01 nm [29]), and $N_A$ is the Avogadro's number. A value of 55.8 (±4.7) nm for the PB thickness layer could be obtained. This value suggests that the equivalent PB thickness is almost fifty times that for a monolayer, which supports the fast kinetic observed in the cyclic voltammetric experiments where the $K^+$ ions diffusion into the PB layer is the limiting factor. On the other hand, it could be asserted that the conversion of PB to ES and back to PB takes place fast in a reversible manner ensuring the full conversion of the PB material into its redox forms. If a thicker layer of PB was present, then a limitation of the charge transfer process could be expected for the diffusion of $K^+$ ions into the PB lattice to ensure the full conversion between the two redox forms of PB/ES system.

These findings are also supported by scanning electron microscopy (SEM) measurements. Figure 2 displays the SEM images recorded for ATO-PB materials at various magnifications. Small grain PB particles can be observed on the surface of ATO microparticles.

The electrochemical properties of ATO-PB electrode material were also investigated by means of electrochemical impedance spectroscopy (EIS). The EIS measurements were performed in 0.1 M KCl solution at applied potentials of 0.14 V vs. $Ag/Ag^+$ and 0.82 V vs. $Ag/Ag^+$, respectively. These potential values correspond to the formal potentials values of the PB/ES and PB/BG redox systems estimated as follows: $E^{0'} = (E_{pa} + E_{pc})/2$. The aim is to investigate the electron transfer capability of the ATO-PB electrode material at applied potential close to the formal potential of the corresponding redox systems. Figure 3 displays the impedance spectra recorded at ATO-PB-SPE device at 0.14 V vs. $Ag/Ag^+$ and 0.82 V vs. $Ag/Ag^+$, respectively.

The EIS spectra were fitted by using an equivalent electrical circuit (inset of Fig. 3) composed of the solution resistance, ($R_s$), the charge transfer resistance ($R_{ct}$) in parallel with the constant phase element (*CPE, Q1*), and a second constant phase element in serie (*CPE, Q2*). The fitted values are displayed in Table 1.

There is a difference between the charge transfer resistance values ascribed to PB/ES (at 0.14 V vs. $Ag/Ag^+$) and PB/BG (at 0.82 V vs. $Ag/Ag^+$) redox systems. There is a 1.5 times increase of the charge transfer resistance for the spectrum at 0.82 V vs. $Ag/Ag^+$, which suggests a slower electron transfer capability compared to the value obtained at the

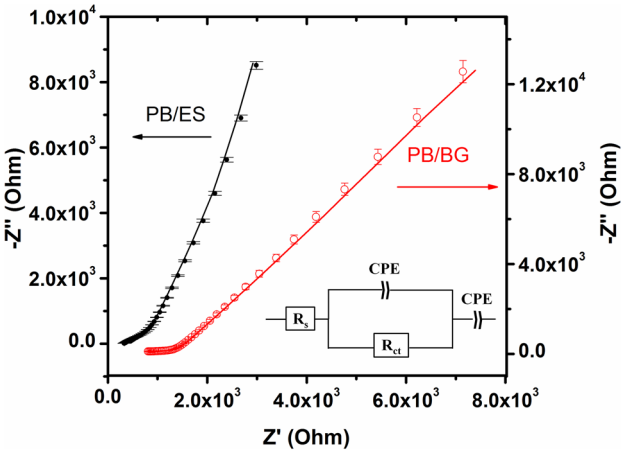


**Fig. 3** EIS spectra recorded at ATO-PB-SPE in 0.1 M KCl aqueous solution at different applied potential values for PB/ES (left Y axis) and PB/BG (right Y axis) redox systems. The continuous lines represent the fitted spectra. Inset: the equivalent electrical circuit used in the fitting of the electrochemical impedance spectra

0.14 V vs. $Ag/Ag^+$ applied potential. The charge transfer process may be ascribed to the electrons hopping between ATO and PB centers. The first constant phase element may be ascribed to the ATO/PB interface, while second constant phase element could be related to the PB/electrolyte interface. This finding underlines the fast charge transfer process of the PB/ES redox system in $K^+$ containing solution and fosters the potential application of this redox system in the electrochemical sensing of $K^+$ ions.

## Analytical applications of ATO-PB-SPE

### Potassium ions detection

The capability of ATO-PB electrode material to detect potassium ions has been investigated by means of cyclic voltammetry in aqueous solution containing various $K^+$ concentrations ranging from 0.1 to 10 mM (see Fig. 4A).

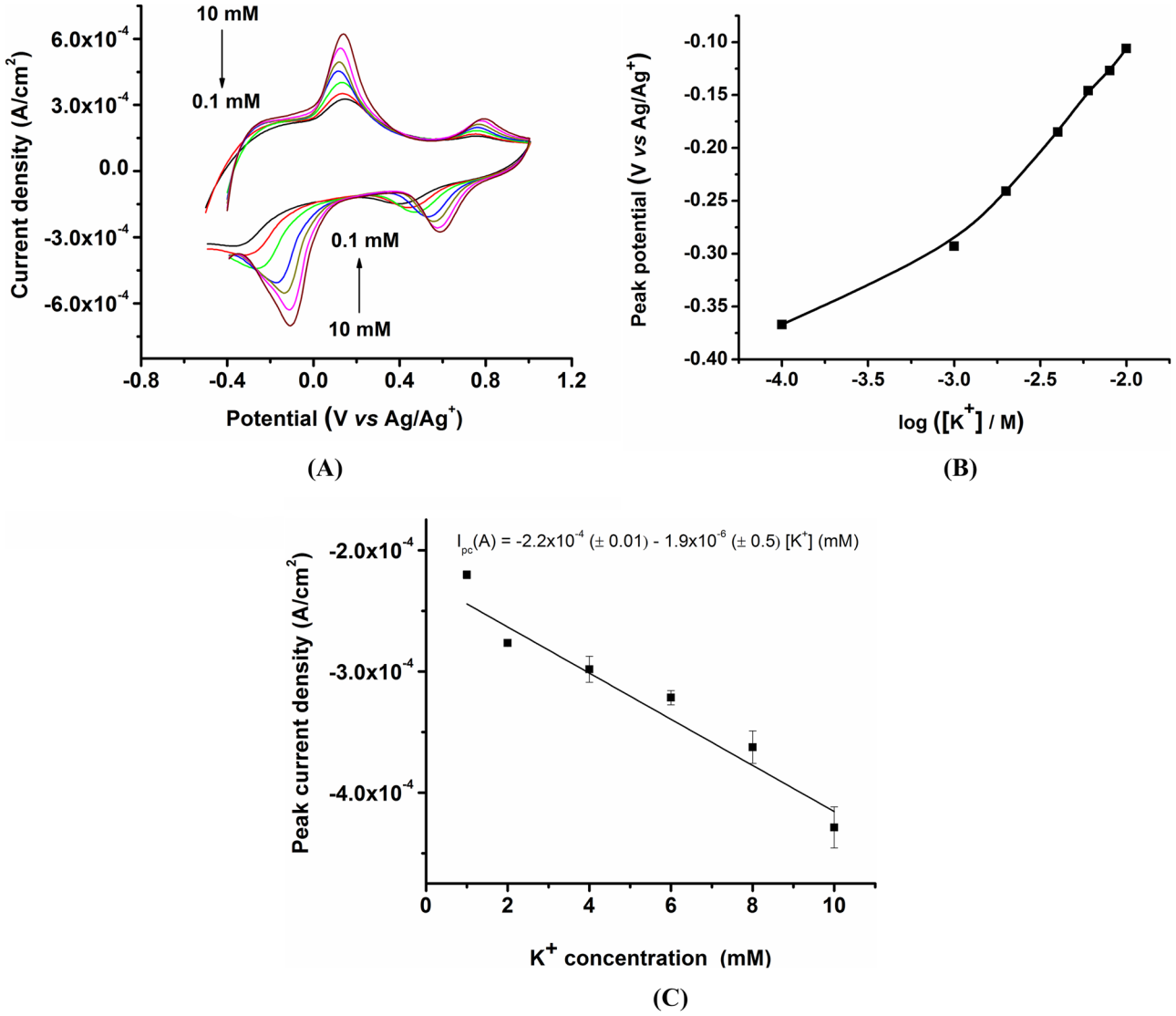


**Fig. 4** **A** CVs recorded at ATO-PB-SPE device in aqueous solutions containing $K^+$ concentrations of 0.1, 1, 2, 4, 6, 8, and 10 mM. Potential scan rate of 50 mV $s^{-1}$. **B** Dependence of the cathodic peak potential on $K^+$ concentration. **C** Linear dependence of the cathodic peak current on $K^+$ concentration.

It can be observed that the cathodic peak current of the PB/ES redox system decreases proportionally to $K^+$ concentrations from 10 to 0.1 mM. A concomitant shift of the cathodic peak potential of the PB/ES system toward less positive potential is also obtained. This behavior is determined by the change in $K^+$ concentrations in the electrolyte solution. The characteristics peak potential and current of the redox wave of PB/ES system are clearly sensitive to this change in $K^+$ concentrations. The cathodic peak potential is decreasing linearly for $K^+$ concentrations ranging from 10 to 1 mM according to the data displayed in the Fig. 4B. The slope of the $E_{pc}$ versus $log\ [K^+]$ plot is of 0.188 V/decade of concentration and it is higher than the theoretical value characteristic to an ion-selective electrode for monovalent ions response attesting the capability of the ATO-PB electrode material to display super-Nernstian response toward the electro-inactive $K^+$ ions. The increased slope value points out to a sensing mechanism that combines both the ion exchange process specific to membrane-based ion-selective electrodes and the electron hoping process involved in the PB/ES redox reaction due to the electrochemical activity of the PB material. The fast and reversible insertion/exclusion of potassium ions into PB layer is a diffusion-controlled process and ensure a full conversion of PB between its reduced and oxidized forms. The small thickness of the PB layer estimated above in Sect. 3.1, attests the rapid attention of the equilibrium within the PB layer. The electron hoping in the PB/BG redox reaction is associated with the exchange process of potassium ions. Thanks to the very high conductivity of the PB material and the rapid exchange process of the potassium ions, the ATO-PB material displays an electrochemical response characterized by an increased slope compared to the theoretical one of 59 mV/decade of concentration for monovalent cations. Actually, there is a large increase of the slope by a factor of 3 compared to the theoretical one for monovalent cations. This large increase of the slope could be ascribed to the combined ion exchange and electron hopping mechanisms of the sensing material. In this way, an increased sensitivity of the sensor's response is obtained that could be advantageous in the discrimination of various samples containing similar $K^+$ ion concentrations. There is also a linear dependence of the cathodic peak current of PB/ES redox wave with the $K^+$ concentrations as depicted in Fig. 4C. The sensitivity calculated from the slope of the $I_{pc}$ versus $K^+$ concentration plot from Fig. 4C is 0.035 A $M^{-1}$ $cm^{-2}$. The limits of detection (LOD) and quantification (LOQ) could be estimated by means of the following criteria: $LOD = 3\ SD/m$, and $LOQ = 10\ SD/m$ where $SD$ is the standard error of the regression line intercept and $m$ is the slope of the cathodic peak current versus $K^+$ concentration plot. Consequently, a LOD value of 1.1 mM and LOQ value of 3.7 mM $K^+$, respectively, have been obtained. The LOQ value is close to the lower limit of the normal level of potassium ions in blood, i.e., from 3.5 to 5.3 mM [30] suggesting the potential application of the sensor in biomedical analysis. The repeatability was estimated by measuring a 10 mM $K^+$ concentration with the same device for three times and expressed as relative standard deviation (RSD%). A value of 14.6% has been obtained.

The selectivity of ATO-PB sensor toward potassium ions over other common interfering species like sodium ions was also investigated. It is known that PB displays the best voltammetric response in potassium containing electrolyte solutions due to the zeolitic structure of PB crystal and the size of potassium ions. Sodium ions are present usually in various samples from bio-medical and food fields together with potassium ions. In this sense, the influence of sodium ions on the response of the ATO-PB sensor was studied. Figure 5A shows the cyclic voltammograms recorded at ATO-PB sensor in potassium-based phosphate solution containing various amounts of NaCl as interfering species.

There is a decrease of the cathodic and anodic currents for both redox waves in the presence of increasing sodium ions concentration and a concomitant shift of the cathodic and anodic potentials toward electropositive values. However, the decrease of the cathodic peak potential of the PB/ES system with sodium ions concentrations is linear over the range from 1 to 10 mM (see Fig. 5B). The slope of the $E_{pc}$ versus $log\ [Na^+]$ plot is of 0.058 V/decade of concentration, a value close to the theoretical one for an ion-selective electrode for monovalent ions. This behavior indicates the that the ATO-PB sensing materials still displays its characteristic redox behavior, but there is a competition between the potassium ions flux into/out of the PB layer the flux in/out of the sodium ions. The sodium ions are replacing the potassium ions from the PB structure and this phenomenon is indicated by the change in the cathodic and anodic currents and potentials of the PB/ES and PB/BG redox waves. The zeolitic structure of the PB crystal strongly influences the electrochemical properties of PB in potassium ions containing solution. The displacement of potassium ions by the sodium ions resulted in the decrease of both the anodic and cathodic peak currents, while the positive shift of the anodic and cathodic peak potential reveals the competition between potassium and sodium ions in the reaction. The initial shape of the redox wave is maintained in the presence of sodium ions, demonstrating a reversible insertion/extraction mechanism of the interfering species. The positive shift of the anodic and cathodic peak potentials reveals that the insertion of sodium ions takes place merely at the surface of the PB layer. This behavior is translated in the Nernstian slope of the cathodic peak potential versus sodium ion concentration plot. Consequently, there is a decrease of the slope of the peak potential versus ion concentration plot compared to that observed in the case of dynamic change of $K^+$ ions concentration (see Fig. 4B). The cathodic peak current of the PB/ES

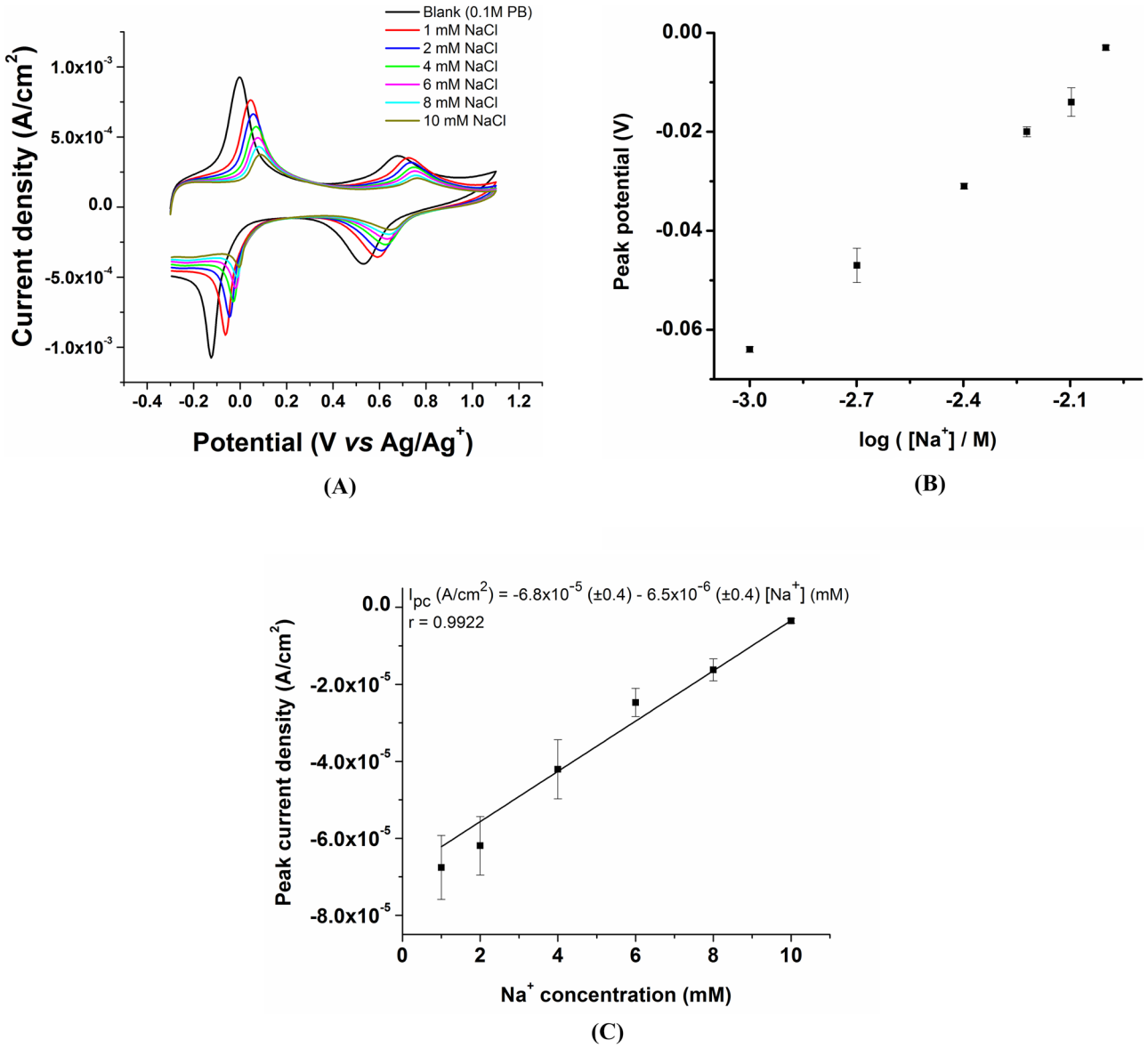


**Fig. 5** **A** CVs recorded at ATO-PB-SPE sensor in 0.1 M potassium phosphate buffer solution (PB) containing added $Na^+$ concentrations of 1, 2, 4, 6, 8, and 10 mM. Potential scan rate of 50 mV $s^{-1}$. **B** Dependence of the cathodic peak potential on $Na^+$ concentration. **C** Linear dependence of the cathodic peak current density on $Na^+$ concentration.

redox wave is decreasing linearly with the increasing sodium ions concentration over the range from 1 to 10 mM (see Fig. 5C). These results regarding the insertion of sodium ions into the PB lattice are suggesting that some interstitial sites are occupied by sodium ions. Consequently, the initial shape of the redox wave is clearly maintained in the presence of sodium ions and this suggests a good stability of the PB layer without a clear dissolution or physical degradation. The ATO-PB material still retains its redox behavior under these experimental conditions despite the linear decrease of the currents and the obtained results could be exploited in the detection of sodium ions in the presence of a large concentration of potassium ions of 0.1 M.

The analytical performance of the ATO-PB based sensor toward potassium ions detection is comparable with that of other electrochemical sensors previously published in literature (Table 2). Actually, there is a limited number of papers dealing with PB-based sensing materials for potassium ion detection. In this sense, the comparison has taken into account other sensing materials including natural receptors for potassium ion like valinomycin. The ease of preparation of ATO-PB electrodes, including the mass production by means of the screen-printing technology for disposable sensors, and the low cost of the sensing materials are undoubtedly important factors that overcome some limitations observed in the case of natural or synthetic ionophore for potassium ions and other

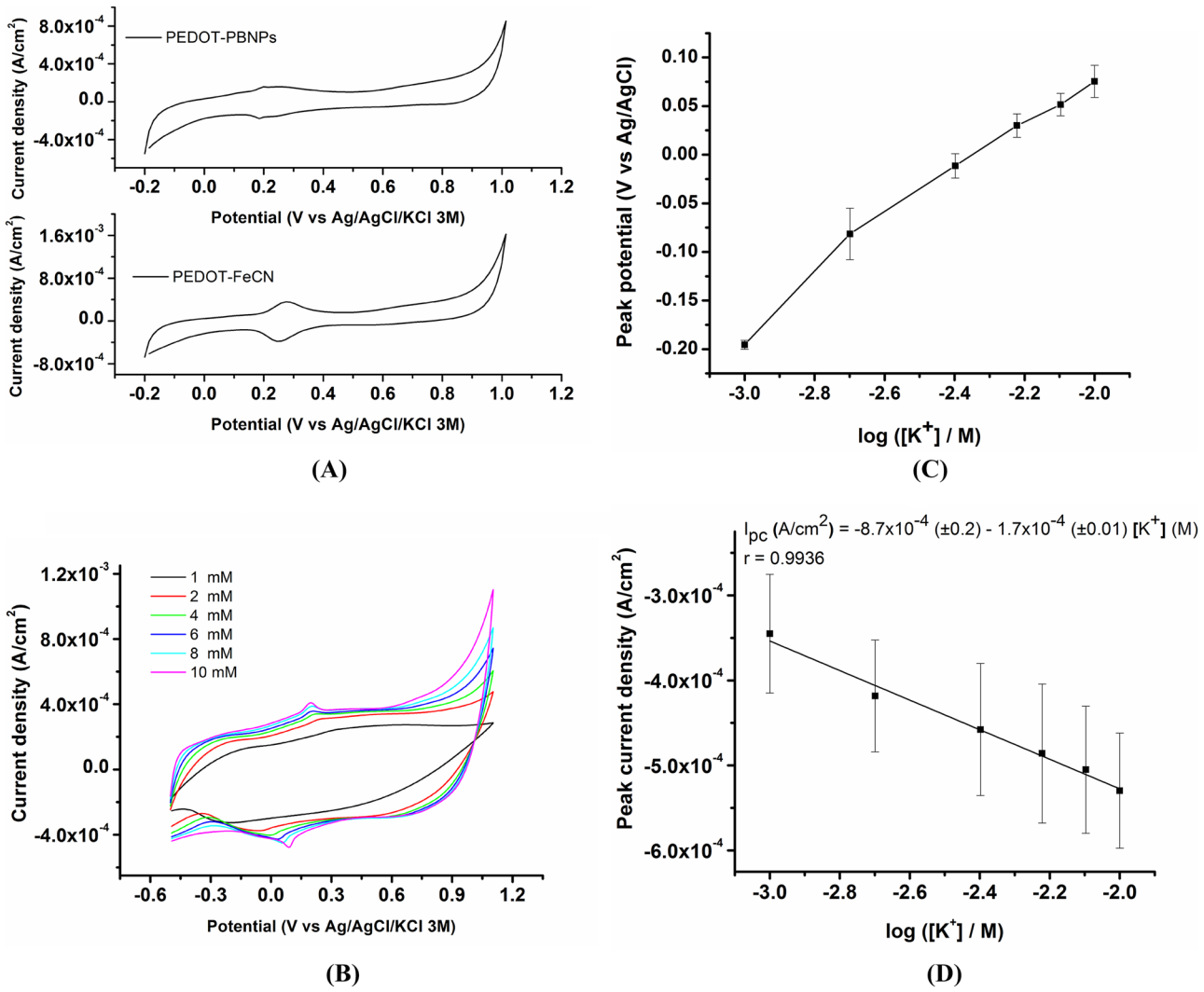


**Fig. 6** **A** CVs recorded in 0.1 M KCl and 0.01 M HCl at PEDOT-FeCN-GCE modified electrode (bottom panel) and PEDOT-PB-GCE sensor (upper panel). Potential scan rate of 50 mV $s^{-1}$. **B** CVs recorded at PEDOT-PB-GCE sensor in the presence of various $K^+$ concentrations of 1, 2, 4, 6, 8, and 10 mM. Potential scan rate of 50 mV $s^{-1}$. **C** Dependence of the cathodic peak potential on $K^+$ concentration. **D** Linear dependence of the cathodic peak current on $K^+$ concentration.

biological recognition elements. In addition, the obtained analytical performance in terms of low detection and quantification limits, near physiological linear response range, high analytical sensitivity, combines very well with the low cost and mass production features into feasible and affordable electrochemical sensors for potassium ions detection.

Therefore, the obtained low detection and quantification limits values and the high value of the sensitivity point out to the potential use of the ATO-PB electrode material as sensing element in the development of an electrochemical sensor for $K^+$ detection.

**Table 1** Fitted values of the EIS spectra

| Applied potential (V vs. $Ag/Ag^+$) | *Rs* (Ω) (±error %) | *Rct* (Ω) (±error %) | $Q1/Y_0$ ($\Omega^{-1}$ $s^{-n}$) (±error %); *n* (±error %) | $Q2/Y_0$ ($\Omega^{-1}$ $s^{-n}$) (±error %); *n* (±error %) |
|---|---|---|---|---|
| 0.14 | 322.4 (±0.4) | 602.3 (±3.4) | $2.1\times10^{-4}$ (±4.7); 0.56 (±1.6) | $2.9\times10^{-4}$ (±0.4); 0.84 (±0.4) |
| 0.82 | 561.4 (±3.6) | 900.0 (±3.5) | $5.8\times10^{-5}$ (±6.1); 0.33 (±3.6) | $1.7\times10^{-4}$ (±0.2); 0.72 (±0.2) |

**Table 2** Comparison of the analytical performances of the ATO-PB based sensor toward potassium ion with those of electrochemical (bio)sensors previously reported in literature

| (Bio)sensor type | Linear Range (M) | LOD (M) | Ref |
|---|---|---|---|
| ATO-PB | $1.0\times10^{-4}$ – $1.0\times10^{-2}$ | $1.1\times10^{-4}$ | [This work] |
| TPE | $1.0\times10^{-4}$ – $1.0\times10^{-1}$ | $1.0\times10^{-4}$ | [31] |
| ISM-RGO/Au electrode | $6.0\times10^{-5}$ – $2.5\times10^{-1}$ | $6.0\times10^{-5}$ | [32] |
| C/MWCNTs-MXene/ valinomycin | $1.0\times10^{-3}$ – $3.2\times10^{-2}$ | - | [33] |
| PB nanotubes | $5.0\times10^{-8}$–$7.0\times10^{-4}$ and $7.0\times10^{-4}$–1.0 | $2.0\times10^{-8}$ | [34] |
| Fc/HRP-DNAzyme | $5.0\times10^{-6}$–$2.0\times10^{-4}$ | $1.6\times10^{-6}$ | [35] |

*ATO-PB* antimony tin oxide-Prussian blue, *TPE* thermoplastic electrode, *ISM-RGO/Au electrode* potassium ion-selective valinomycin membrane deposited onto reduced graphene oxide/Au electrode, *C/MWCNTs-MXene/ valinomycin* carbon-multiwall carbon nanotubes-MXene-valinomycin electrode, *PB nanotubes* Prussian blue nanotubes, *Fc/HRP-DNAzyme* ferrocene unit relay connected to horseradish peroxidase-mimicking enzyme

## Analytical applications of PEDOT-PB-GCE

### Potassium ions detection

The PEDOT-PB-GCE device has been investigated by cyclic voltammetry in aqueous solution containing potassium ions, aiming to obtain information regarding the electrochemical behavior of the composite material, namely the redox activity of the PB component. After the deposition of the PEDOT-FeCN coating by means of the sinusoidal voltage procedure, the modified electrode was transferred in aqueous solution containing 0.1 M KCl and 0.01 M HCl and the cyclic voltammograms were recorded over an extended potential range at a 50 mV $s^{-1}$ potential scan rate. The corresponding cyclic voltammograms are depicted in the bottom panel of the Fig. 6A. There is a redox wave at 0.25 V vs. Ag/AgCl/KCl (3 M) which is characteristic to the ferricyanide ions entrapped within the polymeric PEDOT coating during the electropolymerization process as counter ions to maintain the electroneutrality. After the preparation of the PEDOT layer dopped with ferrocyanide ions, the in situ formation of the PB within the PEDOT layer takes place during the second deposition step by sinusoidal voltage in Fe(III) containing solution. The reduction of Fe(III) to Fe(II) ions resulted in the formation of the PB component. The upper panel of Fig. 6A displays the cyclic voltammogram recorded in the 0.1 M KCl and 0.01 M HCl aqueous solution. The redox wave of PB appears at ca. 0.19 V vs. Ag/AgCl/KCl (3 M) with anodic peak potential of 0.214 V vs. Ag/AgCl/KCl (3 M) and the cathodic peak potential of 0.185 V vs. Ag/AgCl/KCl (3 M). The peak-to-peak potentials difference is of 0.029 V, characteristic to redox species immobilized onto the electrode surface. Furthermore, the second wave related to the PB/BG redox system is not visible under these experimental conditions. However, the presence of the PB/ES redox wave is essential for the sought analytical applications regarding the detection of the potassium ions. Figure 6B displays the cyclic voltammograms recorded at the PEDOT-PB-GCE device in the presence of various $K^+$ concentration ranging from 1 to 10 mM. Both the anodic and cathodic peak currents of the PB/ES redox wave decrease with the potassium ion concentration. Also, the cathodic peak potential of the PB/ES redox wave decreases and shifted to the negative potential values with potassium ion concentration, similarly to the ATO-PB-SPE sensor. This behavior clearly demonstrates the electroactivity of the PB component from the composite materials towards potassium ion. The dependence of the cathodic peak potential on potassium ion concentration is displayed in Fig. 6C. A value of 0.156 V/decade of concentration for the slope of the $E_{pc}$ versus $log\ [K^+]$ plot has been obtained. This value is larger than the theoretical value for monovalent ions and suggests that the sensing mechanism includes the electron hopping transfer process besides the ion-exchange characteristic for membrane based ion-selective electrodes. The value of the slope is closed to that of the ATO-PB-SPE sensor showing comparable analytical characteristic of the two sensing materials.

In addition, a linear dependence of the cathodic peak current of the PB/ES redox system with the potassium ion concentrations has been observed (see Fig. 6D). A sensitivity value of 0.018 A $M^{-1}$ $cm^{-2}$. has been calculated from the slope of the $I_{pc}$ versus $K^+$ concentration plot. The slope value is smaller than that observed for the ATO-PB-SPE sensor and this is corroborated with the amount of PB catalyst in each composite material. It is difficult the control precisely the amount of PB component in each composite material, but the comparison is useful in demonstrating the analytical capability of the PB based sensing materials. A LOD value of 3.1 mM $K^+$ has been obtained which is larger than that of the ATO-PB-SPE device. The repeatability expressed as relative standard deviation (RSD%) has been estimated by measuring a 10 mM potassium ion concentration with the same PEDOT-PB-GCE sensor for three times and a value of 12.8% has been obtained. These results suggest that the low-cost composite materials ATO-PB and PEDOT-PB prepared by a

mass production procedure, the former one, and a laboratory and simply electrochemical procedure, the later one, could have potential applications in the potassium ion detection.

## Conclusions

In this work, the novel ATO-PB and PEDOT-PB electrode materials have been investigated in the electrochemical detection of electro-inactive analytes. The electrochemical properties of ATO-PB electrode material have been investigated by means of cyclic voltammetry and electrochemical impedance spectroscopy. Good electron transfer capability of the PB component has been obtained. The high surface coverage of PB onto ATO nanoparticles enabled good electrochemical and electrocatalytic activity of the ATO-PB electrode material. The cathodic peak potential of the PB/ES redox systems shifted toward less positive potential with the decrease of $K^+$ ions in the contacting electrolyte solution. Also, the cathodic peak current of the PB/ES wave displayed a linear dependence on the $K^+$ ions concentrations over the range from 0.1 to 10 mM. The ATO-PB electrode material was applied in the electrochemical detection of $K^+$ ions, the detection and quantification limits were of 1.1 mM and of 3.7 mM, respectively. The electrochemical sensor displayed also a high sensitivity of 0.035 A $M^{-1}$ $cm^{-2}$. The obtained linear response range and the quantification limit ensures the possible application of the developed sensor in the $K^+$ ions determination in real samples. The PEDOT-PB sensing material was prepared by a novel procedure based on the use of a sinusoidal voltage superimposed on the constant potential. The developed PEDOT-PB sensing material displayed good analytical performance toward the potassium ion detection with a linear response range from 1 to 10 mM and a detection limit of 3.1 mM. These results point out to the potential applications of the ATO-PB electrode material in the electrochemical sensing of electro-inactive analytes.

**Acknowledgements** This work was supported by a grant of the Ministry of Research, Innovation and Digitization, CNCS/CCCDI – UEFISCDI, project number PN-III-P2-2.1-PED-2021-3693, within PNCDI III. JdC gratefully acknowledges funding from the Spanish Research Agency, AEI, (Project number PID2020-113154RB-C22). A part of this work was carried out within the research program "Electrode processes, corrosion and materials for electrochemical systems" of the "Ilie Murgulescu" Institute of Physical Chemistry, Romanian Academy.

**Author contribution** **Sorina Alexandra Leau**: Investigation, Formal Analysis, Data curation, Writing—original draft. **Cecilia Lete**: Conceptualization, Methodology, Supervision, Validation, Investigation, Formal analysis, Writing—original draft, Writing—review & editing. **Mariana Marin:** Formal analysis, Data curation. **Francisco Javier del Campo**: Conceptualization, Investigation, Writing—review & editing. **Ioana Diaconu**: Formal analysis, Data curation, Writing—review & editing. **Stelian Lupu**: Supervision, Conceptualization, Methodology, Validation, Investigation, Data curation, Formal analysis, Resources, Writing—original draft, Writing—review & editing.

## Declarations

**Conflict of interest** The authors declare no competing interests.

## References

1. Arduini F, Micheli L, Moscone D, Palleschi G, Piermarini S, Ricci F, Volpe G (2016) Electrochemical biosensors based on nanomodified screen-printed electrodes: recent applications in clinical analysis. TrAC Trends Anal Chem 79:114–126. https://doi.org/10.1016/j.trac.2016.01.032
2. Hayat A, Marty JL (2014) Disposable screen printed electrochemical sensors: tools for environmental monitoring. Sens Basel 14:10432–10453. https://doi.org/10.3390/s140610432
3. Pérez-Fernández B, Costa-García A, de la Escosura-Muñiz A (2020) Electrochemical (bio)sensors for pesticides detection using screen-printed electrodes. Biosensors 10:32. https://doi.org/10.3390/bios10040032
4. Dhanapala L, Krause CE, Jones AL, Rusling JF (2020) Printed electrodes in microfluidic arrays for cancer biomarker protein detection. Biosensors 10:115. https://doi.org/10.3390/bios10090115
5. Antuña-Jiménez D, González-García MB, Hernández-Santos D, Fanjul-Bolado P (2020) Screen-printed electrodes modified with metal nanoparticles for small molecule sensing. Biosensors 10:9. https://doi.org/10.3390/bios10020009
6. Jiménez-Pérez R, Iniesta J, Baeza-Romero MT, Valero E (2021) On the performance of carbon-based screen-printed electrodes for (in)organic hydroperoxides sensing in rainwater. Talanta 234:122699. https://doi.org/10.1016/j.talanta.2021.122699
7. O'Halloran MP, Pravda M, Guibault GG (2001) Prussian Blue bulk modified screen printed electrodes for $H_2O_2$ detection and for biosensors. Talanta 55:605–611. https://doi.org/10.1016/S0039-9140(01)00469-6
8. Aller Pellitero M, Colina Á, Villa R, Javier del Campo F (2018) Antimony tin oxide (ATO) screen-printed electrodes and their application to spectroelectrochemistry. Electrochem Commun 93:123–127. https://doi.org/10.1016/j.elecom.2018.06.012
9. Santiago S, Aller M, del Campo F, Guirado G (2019) Screen-printable electrochromic polymer inks and ion gel electrolytes for the design of low-power, flexible electrochromic devices. Electroanalysis 31:1664–1671. https://doi.org/10.1002/elan.201900154
10. Harris TGA, Götz R, Wrzolek P, Davis V, Knapp CE, Ly K, Hildebrandt P, Schwalbe M, Weidinger I, Zebger I, Fischer A (2018) Robust electrografted interfaces on metal oxides for electrocatalysis - an in situ spectroelectrochemical study. J Mater Chem A 6:15200–15212. https://doi.org/10.1039/C8TA02983K
11. Müller V, Rathousky J, Fattakhova-Rohlfing D (2014) Covalent immobilization of redox protein within the mesopores of transparent conducting electrodes. Electrochim Acta 116:1–8. https://doi.org/10.1016/j.electacta.2013.10.136
12. Aller-Pellitero M, Fremeau J, Villa R, Guirado G, Lakard B, Hihn JY, Javier del Campo F (2019) Electrochromic biosensors based on screen-printed Prussian Blue electrodes. Sens Actuat B Chem 290:591–597. https://doi.org/10.1016/j.snb.2019.03.100
13. Itaya K, Uchida I, Neff VD (1986) Electrochemistry of polynuclear transition metal cyanides: Prussian blue and its analogues. Acc Chem Res 19:162–168. https://doi.org/10.1021/ar00126a001
14. Neff VD (1978) Electrochemical oxidation and reduction of thin films of Prussian blue. J Electrochem Soc 128:886–887. https://doi.org/10.1149/1.2131575

15. Itaya K, Ataka T, Toshima S (1982) Spectroelectrochemistry and electrochemical preparation method of Prussian blue modified electrodes. J Am Chem Soc 104:4767–4772. https://doi.org/10.1021/ja00382a006
16. Karyakin AA, Karyakina EE, Gorton L (1996) Prussian Blue based amperometric biosensors in flow-injection analysis. Talanta 43:1597–1606. https://doi.org/10.1016/0039-9140(96)01909-1
17. Karyakin AA (2001) Prussian Blue and its analogues: electrochemistry and analytical applications. Electroanal 13:813–819. https://doi.org/10.1002/1521-4109(200106)13:10%3c813::AID-ELAN813%3e3.0.CO;2-Z
18. Ricci F, Palleschi G (2005) Sensor and biosensor preparation, optimisation and applications of Prussian Blue modified electrodes. Biosens Bioelectron 21:389–407. https://doi.org/10.1016/j.bios.2004.12.001
19. Marquitan M, Clausmeyer J, Actis P, Cordoba AL, Korchev Y, Mark MD, Herlitze S, Schuhmann W (2016) Intracellular hydrogen peroxide detection with functionalised nanoelectrodes. ChemElectroChem 3:2125–2129. https://doi.org/10.1002/celc.201600390
20. Karyakin AA (2017) Advances of Prussian blue and its analogues in (bio)sensors. Curr Opin Electrochem 5:92–98. https://doi.org/10.1016/j.coelec.2017.07.006
21. Xu Y, Zheng S, Tang H, Guo X, Xue H, Pang H (2017) Prussian blue and its derivatives as electrode materials for electrochemical energy storage. Energy Storage Materials 9:11–30. https://doi.org/10.1016/j.ensm.2017.06.002
22. Celiesiute R, Ramanaviciene A, Gicevicius M, Ramanavicius A (2019) Electrochromic sensors based on conducting polymers, metal oxides, and coordination complexes. Crit Rev Anal Chem 49:195–208. https://doi.org/10.1080/10408347.2018.1499009
23. Cinti S, Cusenza R, Moscone D, Arduini F (2018) Paper-based synthesis of Prussian Blue nanoparticles for the development of whole blood glucose electrochemical biosensor. Talanta 187:59–64. https://doi.org/10.1016/j.talanta.2018.05.015
24. Tomei MR, Cinti S, Interino N, Manovella V, Moscone D, Arduini F (2019) Paper-based electroanalytical strip for user-friendly blood glutathione detection. Sens Actuat B Chem 294:291–297. https://doi.org/10.1016/j.snb.2019.02.082
25. Ortiz-Aguayo D, De Wael K, del Valle M (2021) Voltammetric sensing using an array of modified SPCE coupled with machine learning strategies for the improved identification of opioids in presence of cutting agents. J Electroanal Chem 902:115770. https://doi.org/10.1016/j.jelechem.2021.115770
26. Aller-Pellitero M, Santiago-Malagón S, Ruiz J, Alonso Y, Lakard B, Hihn JY, Guirado G, Javier del Campo F (2020) Fully-printed and silicon free self-powered electrochromic biosensors: Towards naked eye quantification. Sens Actuat B Chem 306:127535. https://doi.org/10.1016/j.snb.2019.127535
27. Santiago-Malagon S, Río-Colín D, Azizkhani H, Aller-Pellitero M, Guirado G, Javier del Campo F (2021) A self-powered skin-patch electrochromic biosensor. Biosens Bioelectron 175:112879. https://doi.org/10.1016/j.bios.2020.112879
28. Coleman JP, Lynch AT, Madhukar P, Wagenknecht JH (1999) Printed, flexible electrochromic displays using interdigitated electrodes. Sol Energy Mater Sol Cells 56:395–418. https://doi.org/10.1016/S0927-0248(98)00144-5
29. Malik MA, Kulesza PJ, Wlodarczyk R, Wittstock G, Szargan R, Bala H, Galus Z (2005) Formation of ultra-thin prussian blue layer on carbon steel that promotes adherence of hybrid polypyrrole based protective coating. J Solid State Electrochem 9:403–411. https://doi.org/10.1007/s10008-005-0654-x
30. Palmer BF (2015) Regulation of potassium homeostasis. Clin J Am Soc Nephrol 10:1050–1060. https://doi.org/10.2215/CJN.08580813
31. Ozer T, Henry CS (2022) All-solid-state potassium-selective sensor based on carbon black modified thermoplastic electrode. Electrochim Acta 404:139762. https://doi.org/10.1016/j.electacta.2021.139762
32. Yoon JH, Park HJ, Park SH, Lee KG, Choi BG (2020) Electrochemical characterization of reduced graphene oxide as an ion-to-electron transducer and application of screen-printed all-solid-state potassium ion sensors. Carbon Letters 30:73–80. https://doi.org/10.1007/s42823-019-00072-6
33. Zhang S, Zahed MA, Sharifuzzaman Md, Yoon S, Hui X, Barman SC, Sharma S, Yoon HS, Park C, Park JY (2021) A wearable battery-free wireless and skin-interfaced microfluidics integrated electrochemical sensing patch for on-site biomarkers monitoring in human perspiration. Biosens Bioelectron 175:112844. https://doi.org/10.1016/j.bios.2020.112844
34. Thanh Nguyen BT, Ang JQ, Toh CS (2009) Sensitive detection of potassium ion using Prussian blue nanotube sensor. Electrochem Commun 11:1861–1864. https://doi.org/10.1016/j.elecom.2009.08.003
35. Wang G, Chen L, Zhu Y, He X, Xu G, Zhang X (2014) Development of an electrochemical sensor based on the catalysis of ferrocene actuated hemin/G-quadruplex enzyme for the detection of potassium ions. Biosens Bioelectron 61:410–416. https://doi.org/10.1016/j.bios.2014.05.052